

CFD analysis for thermal performance augmentation of solar air heater using deflector ribs

R. Venkatesh¹, N. Kumar², N. Madhwesh², and M.S. Manjunath^{2*}

¹ School of Engineering and IT, Manipal Academy of Higher Education, Dubai campus, G04, DIAC-345050, Dubai UAE

² Department of Mechanical and Manufacturing Engineering, Manipal Institute of Technology, Manipal Academy of Higher Education, Manipal 576104, Karnataka, India

Phone: +91 9483426391

ABSTRACT – This paper presents the effect of deflector ribs on the thermal performance of flat plate solar air heater using Computational Fluid Dynamics (CFD) methodology. The analysis is carried out using two-dimensional computational domain for the Reynolds number range of 6000-18000. RNG k- ϵ turbulence model is used to capture the turbulence characteristics of the flow. The deflector rib has a cross-section of isosceles triangle and is placed transversely with respect to the flow. The distance between consecutive ribs is varied as 40mm, 80mm, 160mm and 320mm while the air gap height is varied as 2mm, 3mm, 5mm and 10mm. The numerical model is validated against the well-known correlation of Dittus-Boelter for smooth duct. The simulation results reveal that the presence of deflector ribs provide augmented heat transfer through flow acceleration and enhanced turbulence levels. With reference to smooth duct, the maximum achieved heat transfer improvement is about 1.39 times for the inter-rib distance of 40mm and an air gap height of 3mm while the maximum friction factor achieved was about 3.82 times for pitch value of 40mm and air gap height of 3mm. The highest thermal enhancement factor is achieved for the pitch value of 320mm and an air gap height of 3mm at Re=6000. The air gap height value of 10mm exhibits thermal enhancement factor values lesser than 1.0 and hence is not recommended for use as heat transfer enhancement device for the entire Reynolds number range used in the analysis. The pitch value of 320 mm exhibits thermal enhancement factor greater than 1.0 for almost all the Reynolds number range used in the analysis and varies between 0.93 and 1.07.

ARTICLE HISTORY

Revised: 06th Mar 2020

Accepted: 22nd Mar 2020

KEYWORDS

Solar air heater;

CFD;

turbulence;

deflector ribs;

Nusselt number

INTRODUCTION

Flat plate solar air heaters are widely used for drying applications in agricultural sector as well as food Industry. It also has huge potential in building space heating which could help reduce the building energy demand. However, flat plate solar air heaters typically operate at lower thermal efficiency owing to higher heat losses as well as poor heat transfer capability of air. Several studies have been undertaken in the past to achieve higher heat transfer in flat plate solar air heaters such as using turbulators, packed bed, fins, multi-pass arrangement, corrugations etc. Use of turbulators have been found to be very common in the literature owing to its simplicity and passive nature of the device where the focus was on disturbing the laminar boundary layer through flow separation and reattachment and significant performance enhancement has been reported in the literature. Ansari and Bazargan [1] conducted optimization study of solar air heater fitted with turbulators using genetic algorithm. They developed semi empirical correlations that were validated against experimental results. They found that use of ribs improves thermal efficiency by about 9% at low Reynolds number conditions. A combination of turbulators and double pass flow arrangement was used by Abdullah et al. [2] to evaluate the thermal performance. Aluminium cans were used as turbulators in staggered as well as in-line arrangement with respect to the flow. They achieved a thermal efficiency as high as 68% for staggered arrangement. Singh et al. [3] used multiple broken ribs for a relative pitch of 10, relative height of 0.043 and achieved a maximum improvement of about 3.24 times that of smooth duct while the friction factor increased by about 3.85 times. Multiple V-shaped ribs provide much improved performance as compared to transverse V-shape as reported by Jin et al. [4]. They made use of Computational Fluid Dynamics (CFD) methodology and found that the highest thermal enhancement factor was about 2.35 times and the rib geometrical parameters are reported to affect the performance. Komolafe et al. [5] recently conducted experiments using rectangular ribs which exhibited a thermal efficiency ranging between 14% and 56%. Use of CFD methodology has been very popular in the thermal design of air heaters in the last few decades. Kumar et al. [6] numerically evaluated the effectiveness of triangular duct solar air heater using chamfered rectangular ribs. They compared the CFD results against the Blasius equation and Dittus-Boelter equation and extended the validated CFD model for the case involving the ribs. They found that the maximum achievable increase in heat transfer is about 2.88 times in terms of Nusselt number. Thakur et al. [7] made use of hyperbolic ribs which have been shown to enhance heat transfer by reducing hotspots generated by entrapped eddies at the rib base corners. Manjunath et al. [8] have shown that

the use of U-shaped rib further enhances the thermal performance of circular ribs by reducing the formation of hot spots at the rib corners.

S-shaped baffles [9] have also been reported to enhance heat transfer considerably through turbulence augmentation. Use of corrugated absorber plate has also been reported such as sinusoidal corrugation [10], V-corrugation [11] and slit-perforated corrugation [12]. The sinusoidal corrugation achieved an increase of about 12.5% thermal efficiency as compared to smooth duct owing to significant flow disturbances underneath the absorber plate due to corrugations. However, the pressure energy losses have also been found to be higher and therefore are suitable at low flow rate conditions. The slit-perforated corrugation provides higher heat transfer area as well as jet impingement through the slits which enhance effective thermal performance as high as 68% as compared to transpired collector and is highly suitable for space heating applications. Curved delta shaped vortex generators [13] have been shown to provide vigorous mixing in air flow. It has been shown that a highest increment factor of 2.26 is possible with the use of perforated curved delta shaped winglets. It has also been shown that perforated rectangular winglets [14] yield a maximum heat transfer of 6.78 times that of smooth duct with a thermal performance factor of 2.01. The concept of porous solar air heater has been adopted by Rajarajeswari et. al. [15] where a porous absorber is made use of consisting of wire screen matrix having various diameter, porosity and pitch. A maximum thermal efficiency of 20% has been reported based on the CFD simulation study. A new concept of helical channelling is used by Heydari and Mesgarpour [16] in a triangular channel which ensures greater contact of air with heated surface thereby providing increased thermal efficiency by about 14.7% with reference to the smooth duct. Attachment of pin fins [17] on receiver plate has been shown to improve thermal efficiency by about 14.2% with a maximum effective efficiency of about 73%. Pin fin arrays have been shown to provide increased area along with fluid mixing around the fins which augment the heat transfer for the Reynolds number range of 4000-24000. While most of the studies focussed on attached rib turbulators, there have been very limited study on the use of detached ribs for heat transfer enhancement. Tsia and Hwang [18] were among the earlier researchers to have reported the use of detached ribs in a rectangular duct. They made use of combination of normal and detached ribs for turbulent flow through a rectangular duct and found that the combination provides improved heat transfer with acceptable pressure loss in the air flow. The flow rates used in their experimental analysis was in the range of 12000-70000. Yongsiri et al. [19] made use of detached ribs in a rectangular channel for the Reynolds number ranging between 4000 and 24000. The angle of the rib with respect to the flow was varied between 0° and 165°. Through CFD simulation study, they found that the angles of 60° and 120° provide improved heat transfer as compared to other angles used in the analysis and the inclination becomes insignificant as the Reynolds number decreases.

Thus, there is an opportunity to improve heat transfer with the use of detached ribs with acceptable pressure loss penalty. However, there have been very limited works reported in the literature with reference to the use of detached ribs and there is a need to study the effect of detached ribs on heat transfer augmentation, especially for flat plate solar air heater applications. The term detached rib is renamed as deflector ribs in this work as it is more appropriate from the viewpoint of its influence on the flow. This paper presents a novel concept of using isosceles triangular sectioned transversely placed flow deflector ribs which divert the flow onto the air heater plate causing flow impingement effect. The effect of pitch as well as the air gap height on the thermal behaviour of solar air heater is evaluated using two dimensional CFD analysis.

CFD ANALYSIS

Assumptions

The analysis involves two dimensional CFD simulation study of solar air heater system in the presence of deflector plates having triangular cross-section for the varying flow rates and constant heat flux conditions. The flow is assumed to be smooth, steady, incompressible and turbulent within the range of operating conditions used in the analysis. The thermo-physical properties of air are assumed to vary insignificantly within the operating conditions used in the analysis as the bulk temperature variation of air is expected to be not more than 3°C to 4°C. The air temperature is assumed to be 300 K at the air duct entry which is same as the assumed ambient temperature and the ambient pressure is taken as 101325 Pa throughout the analysis.

Selection of Computational Domain

CFD methodology is used in the analysis to determine the efficacy of deflector ribs in providing improved heat transfer. Selection of appropriate computational domain in which the flow field is desired to be established is a vital step in any CFD methodology. Owing to geometric and thermal symmetry of the rectangular duct, the CFD study is done by choosing the two-dimensional mid-sectional plane of the rectangular air duct.

The two-dimensional computational domain of smooth air duct used for the CFD simulation study is shown in Figure 1(a). The inlet and exit section lengths of the air duct are selected as per the ASHRAE standards [20] to ensure fully developed turbulent flow and the height of duct is selected as 20 mm. The hydraulic diameter of the duct is found to be 33.33mm. The computational domain of solar air heater with flow deflectors is shown in Figure 1(b). The flow deflectors have the cross-section of an isosceles triangle with a base length of 10 mm and an altitude of 3mm as shown in Figure 1(c). The triangular geometry is selected so as to provide a converging inlet for incoming air and which deflects the air

towards the absorber plate while the diverging outlet provides a gradual exit for air flow. The distance between the ribs is varied as 40mm, 80mm, 160mm and 320mm while the air gap height (H) is varied as 2mm, 3mm, 5mm and 10mm.

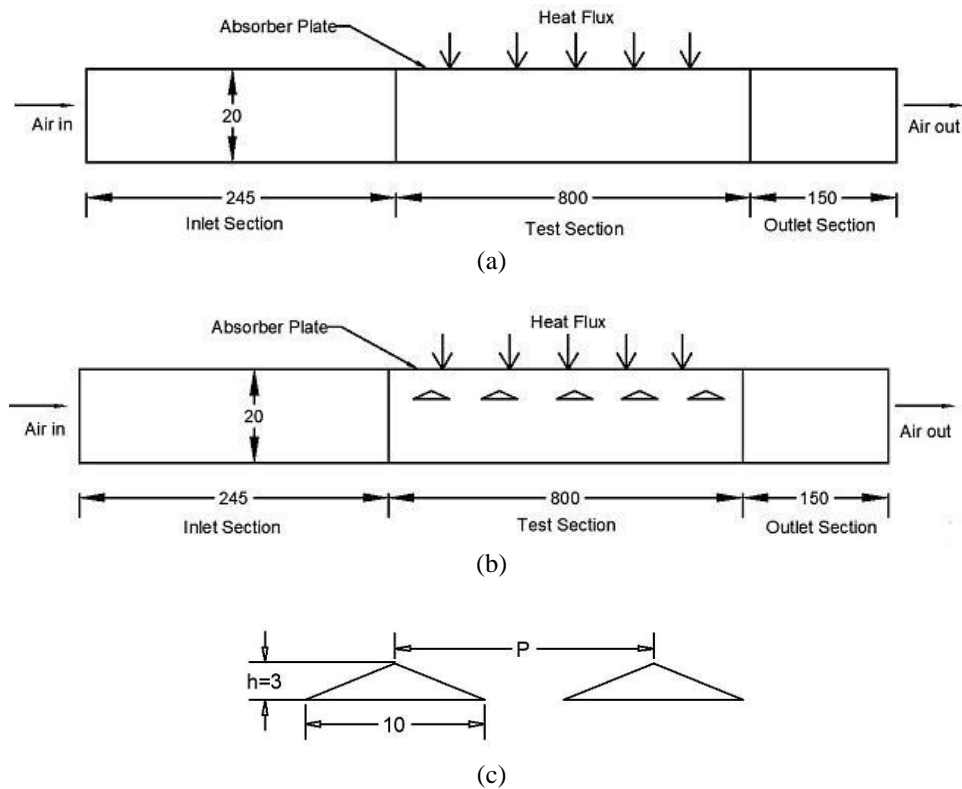


Figure 1. Schematic diagram of: (a) two-dimensional computational domain of solar air heater with smooth duct (b) with deflector ribs and (c) close-up view of deflector geometry (all dimensions in mm)

Governing Equations

The two-dimensional equations of continuity, momentum and energy is given below:

Continuity equation:

$$\frac{\partial}{\partial x_i}(\rho u_i) = 0 \tag{1}$$

Momentum equation:

$$\frac{\partial}{\partial x_i}(\rho u_i u_j) = -\frac{\partial p}{\partial x_j} + \frac{\partial}{\partial x_j} \left[\mu \left\{ \frac{\partial u_i}{\partial x_j} + \frac{\partial u_j}{\partial x_i} \right\} \right] + \frac{\partial}{\partial x_i}(\rho u'_i u'_j) \tag{2}$$

Energy equation:

$$\frac{\partial}{\partial x_i}(\rho u_i T) = \frac{\partial}{\partial x_j} \left[(\Gamma + \Gamma_t) \frac{\partial T}{\partial x_j} \right] \tag{3}$$

where, $p, u, T, \Gamma, \Gamma_t, \rho, u'$ refers to the pressure, velocity, temperature, molecular thermal diffusivity, turbulent thermal diffusivity, density and instantaneous velocity of air respectively.

The RNG $k-\epsilon$ turbulence model equations are as below:

$$\frac{\partial}{\partial x_i}(\rho k u_i) = \frac{\partial}{\partial x_j} \left[\alpha_k \mu_e \left\{ \frac{\partial k}{\partial x_j} \right\} \right] + G_k - \rho \epsilon \tag{4}$$

$$\frac{\partial}{\partial x_i}(\rho \epsilon u_i) = \frac{\partial}{\partial x_j} \left[\alpha_\epsilon \mu_e \left\{ \frac{\partial \epsilon}{\partial x_j} \right\} \right] + C_{1\epsilon} \frac{\epsilon}{k} G_k - R_\epsilon C_{2\epsilon} \rho \frac{\epsilon^2}{k} \tag{5}$$

where, G_k is the turbulent kinetic energy generation given by:

$$G_k = -\frac{\partial u_j}{\partial x_i}(\rho \overline{u'_i u'_j}) \tag{6}$$

The effective turbulent viscosity is given by:

$$\mu_t = C_\mu \rho \frac{k^2}{\epsilon} \quad (7)$$

where, k , ϵ are the turbulent kinetic energy and turbulent kinetic energy dissipation rate respectively and $C_{1\epsilon}$, $C_{2\epsilon}$, C_μ , α_k , α_ϵ are constants given by,

$$C_{1\epsilon} = 1.42, C_{2\epsilon} = 1.68, C_\mu = 0.0845, \alpha_k = 1.39, \alpha_\epsilon = 1.39$$

CFD Solver Settings

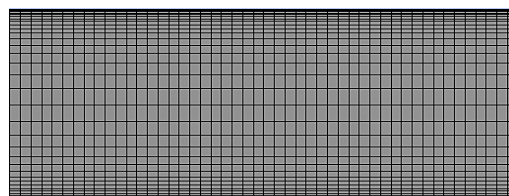
ANSYS Fluent software is used for the simulation study and the correct solver settings is vital for the accuracy of the solution. A known flow velocity varying from 2.86 m/s to 8.65 m/s which falls within the Reynolds number range of 6000 to 18000 is used as inlet boundary condition. A known pressure value of 101325 N/m² is used for the outlet boundary while all other boundaries are assumed as insulated walls in the simulation study. A constant heat flux value of 1000 W/m² is applied on the absorber plate surface to simulate the solar radiation heat flux which varies between 900 W/m² and 1200 W/m² during peak times of the day in most locations. The governing equations of the flow are discretised using second order upwind schemes and a residual of 10⁻⁵ was used as the convergence criteria. SIMPLE algorithm was used for pressure-velocity coupling and RNG k- ϵ turbulence model was adopted in the analysis as suggested by previous researchers [21, 22]. They conducted simulations to compare the Nusselt number values of different turbulence models such as Standard k- ϵ , Renormalisation Group (RNG) k- ϵ , Realizable k- ϵ , Standard k- ω and Shear Stress Transport (SST) k- ω with reference to the Dittus-Boelter correlation for smooth duct flow. They have reported that the Renormalisation Group (RNG) k- ϵ turbulence model predicts the Nusselt number close to that of Dittus-Boelter correlation as compared to other models. Therefore, Renormalisation Group (RNG) k- ϵ turbulence model is adopted in the present analysis.

Grid Independence Study

A grid sensitivity test is done on the smooth duct to determine the optimal mesh for the computational domain. The CFD model for smooth duct is meshed using finer control volumes at the solid-fluid interface to capture the wall effects as shown in Figure 3(a). Table 1 lists the Nusselt number obtained for increasing number of control volumes with the corresponding relative change in Nusselt number. It is seen that the change in Nusselt number is about 0.02% as the number of control volumes increase from 35455 to 420650. Thus, the computational domain is meshed to contain at least 259000 number of control volumes for the simulation study. For the case of air ducts having deflector ribs, finer control volumes are added in the clearance region between the absorber plate and deflector ribs to capture the steep flow gradients as shown in Figure 3(b).

Table 1. Grid independence test results

Number of Control Volumes	Nusselt Number	Percentage Variation (%)
35455	57.01	-
84460	55.46	2.71
125000	58.18	4.92
259000	54.97	5.53
420650	54.95	0.02



(a)

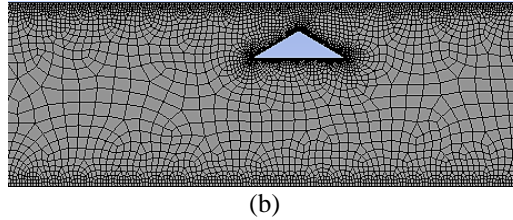


Figure 3. Mesh details for: (a) smooth duct and (b) duct with deflector rib

Validation of the CFD Result

The Nusselt number obtained from the CFD simulation for smooth duct are compared against the Nusselt number values of the well-known Dittus-Boelter equation as shown in Figure 4 for different flow Reynolds number. It is seen that the CFD results match closely with that of Dittus-Boelter equation and the average deviation is about 9.2% thereby giving greater confidence level on the CFD result brought out in the analysis. The Dittus-Boelter equation is given by:

$$Nu = 0.023Re^{0.8}Pr^{0.4} \quad (8)$$

where, Nu is the Nusselt number, Pr is the Prandtl number and Re is the Reynolds number of the flow.

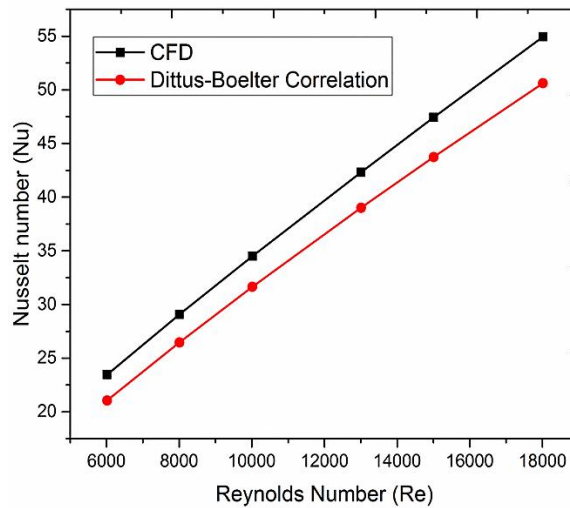


Figure 4. Validation of CFD results for smooth duct.

RESULTS AND DISCUSSION

The effect of pitch variation of deflector rib for a fixed air gap height and the effect of variation of air gap height for a fixed pitch value is evaluated for different Reynolds number and the results are presented with reference to smooth duct. The Nusselt number, friction factor and thermal enhancement factor are brought out to quantify the performance of various configurations of deflector rib.

Effect of Pitch Variation on Heat Transfer Characteristics

The variation of Nusselt number for different pitch values of deflector rib for different flow Reynolds number is shown in Figure 5. The Nusselt number value obtained in the presence of deflector rib are also compared against that of smooth duct. It is seen that the presence of deflector rib generally leads to augmented heat transfer as shown by a relatively higher values of Nusselt number for deflector ribs with reference to smooth duct. It is also seen that lower pitch values produce greater heat transfer. This is due to the fact that lower pitch values lead to the presence of greater number of deflector ribs which provides increased flow disturbances as compared to higher pitch values. The presence of deflector rib leads to significant flow disturbances as shown by the velocity contour plots in Figure 6. The contour plots in Figure 6 is shown for the non-dimensional test section length of $X/L=0.025$ to $X/L=0.15$, where 'L' is the length of the test section and 'X' is the distance along the test section of air duct.

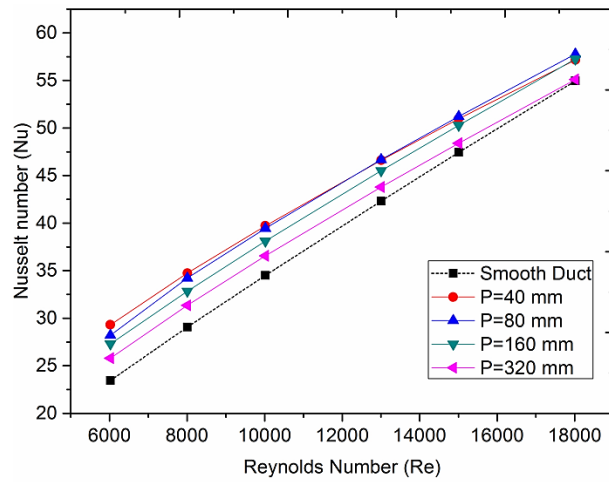


Figure 5. Comparison of Nusselt number for different deflector rib pitch values and a fixed air gap height of 3 mm

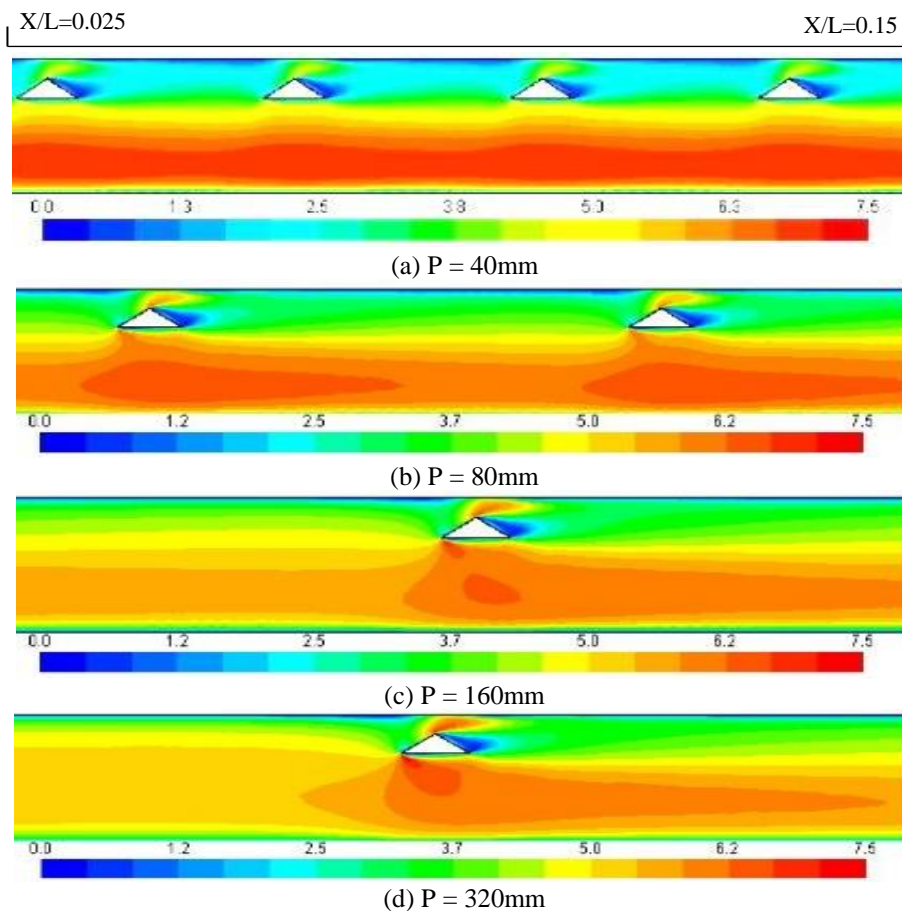


Figure 6. Comparison of velocity contour plots for different pitch values at a fixed height of 3mm for the non-dimensional test section length of X/L=0.025 to X/L=0.15

The deflector rib partly deflects the flow near the absorber plate and force the air to flow through the clearance between the deflector rib and heater plate thereby creating flow acceleration in the air gap. The flow acceleration through the air gap leads to impingement effect thereby providing increased cooling effect. The flow acceleration is clearly indicated within the air gap between the absorber plate and deflector rib in Figure 6.

In addition to this, it is also observed that there is increased fluid interaction on the immediate downstream of each deflector rib which leads to vigorous fluid mixing and hence increased heat energy exchange in the flow. This is clearly indicated by augmented turbulence intensity levels in Figure 7 which shows the contour plots of turbulence intensity. It is seen that the turbulence level on the downstream side of rib is more or less same for different pitch values and there are more number of such locations of augmented turbulence levels with decreasing pitch values.

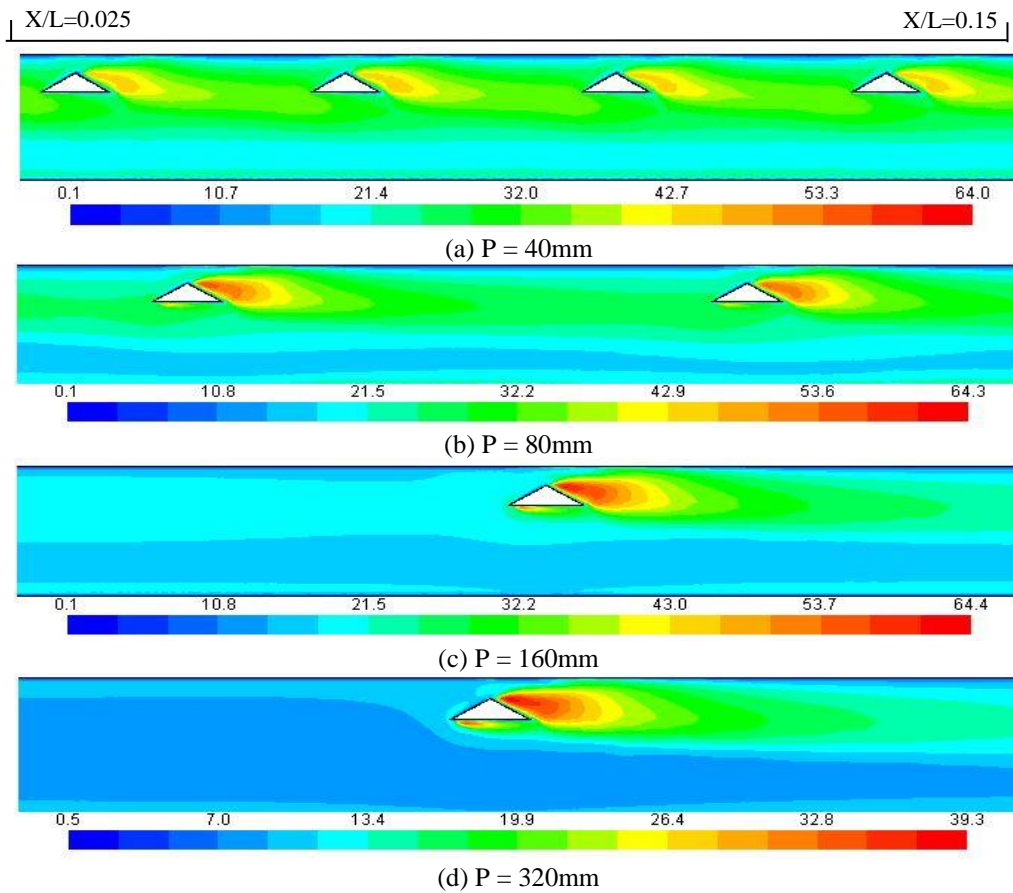


Figure 7. Comparison of turbulence intensity for different pitch values and a fixed height of 3mm for the non-dimensional test section length of $X/L=0.025$ to $X/L=0.15$

This is further evidenced in Figure 8 which shows the comparison of heat transfer co-efficient along the absorber plate for non-dimensional distance of the absorber plate between two consecutive deflector ribs. It is seen that for a lower pitch value of 40mm, the number of locations of peak heat transfer co-efficient are relatively higher as compared to the pitch value of 320mm. The second set of peak locations of heat transfer co-efficient as seen in Figure 8 indicates the regions of enhanced flow mixing on the downstream side of ribs. Thus, the flow acceleration effect and augmented turbulence levels are responsible for providing increased heat transfer as indicated by a relatively higher value of Nusselt number in the presence of deflector rib.

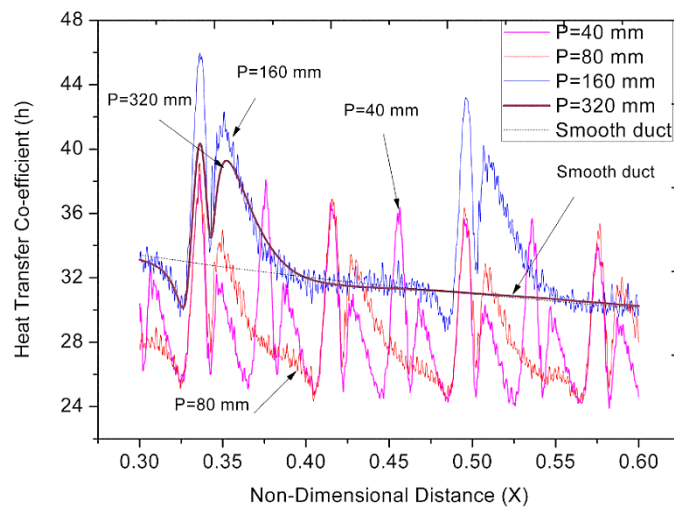


Figure 8. Comparison of heat transfer coefficient for non-dimensional distance of the absorber plate between two consecutive deflector ribs

Effect of Pitch Variation on Friction Factor Characteristics

The influence of pitch variation on friction factor at different Reynolds number is shown in Figure 9 with reference to the friction factor values of smooth duct. The friction factor is evaluated using the Eq. (9):

$$f = \frac{\Delta p D_h}{2\rho LV^2} \tag{9}$$

where, D_h , L and V are the hydraulic diameter of the air duct, length of duct and air velocity in the duct respectively. It is observed that the presence of deflector rib leads to increased friction factor as they offer increased flow obstruction. The flow obstruction is much higher for lower pitch values as there are relatively more number of deflector ribs. The highest friction factor was found to be about 3.82 times higher with reference to smooth duct for a pitch value of 40mm.

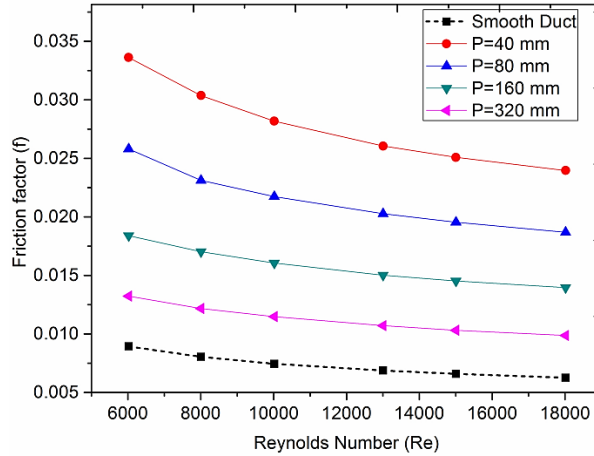


Figure 9. Comparison of friction factor for different pitch values of deflector rib at a fixed air gap height of 3mm.

Effect of Air Gap Height Variation on Heat Transfer Characteristics

The effect of variation of air gap height for a fixed pitch value of 160mm with reference to smooth duct is shown in Figure 9. The Nusselt number variation is insignificant as the height increases from 2mm to 5mm. However, for the height of 10mm, the effect is more pronounced and greater increase in Nusselt number is observed. This is due to the fact that greater height values create increased flow disturbances as shown in Figure 10 which shows the variation of velocity contour plot for different air gap heights of deflector ribs for a fixed pitch value of 160mm.

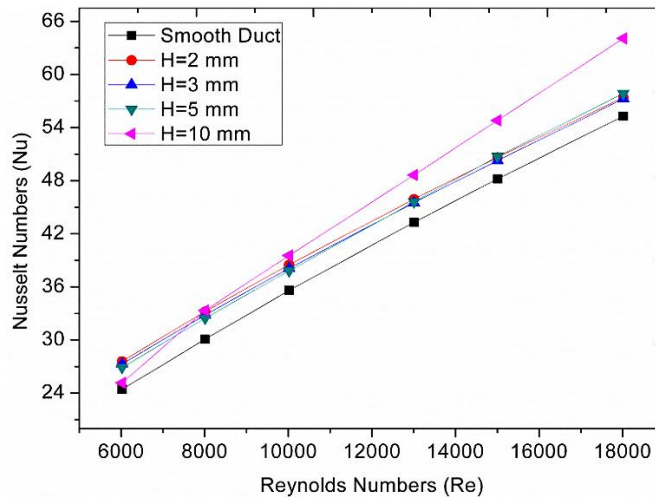


Figure 9. Comparison of Nusselt number for different air gap height values for a fixed deflector rib pitch of 160 mm

It is observed that as the air gap height increases the deflector rib is shifted farther from the absorber plate thereby putting the deflector rib much closer to the core flow where the flow velocities are relatively higher. As a result, at the air gap height value of 10mm, the rib is halfway into the air duct facing the core flow and deflect relatively higher velocity air towards the absorber plate region as shown in Figure 10(d). This creates greater cooling effect on the absorber plate due to its contact with relatively fast moving and colder core flow thereby increasing the heat transfer.

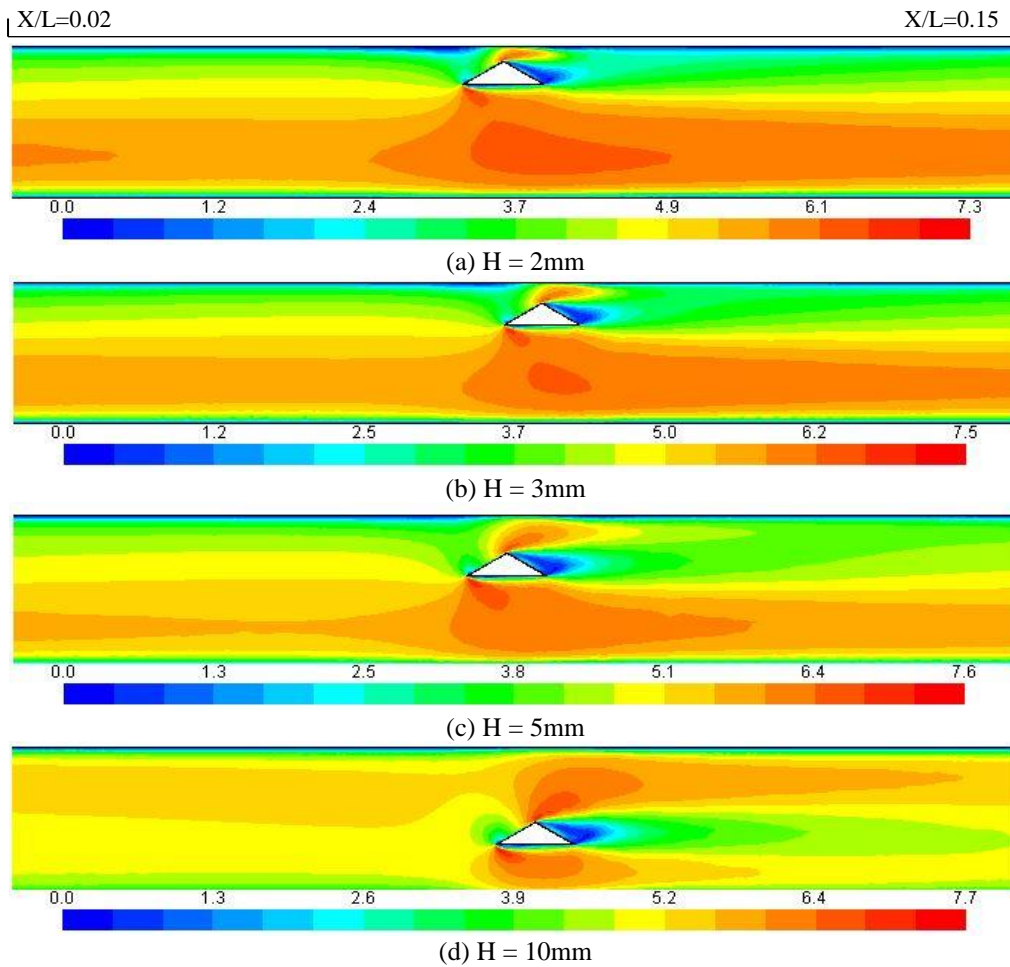
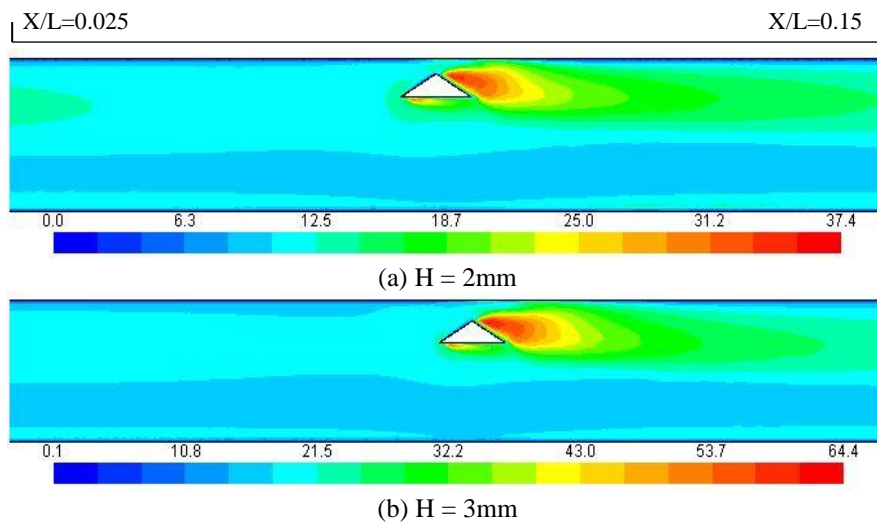


Figure 10. Comparison of velocity contour plots for different heights at a fixed pitch value of 160 mm for the non-dimensional test section length of $X/L=0.025$ to $X/L=0.15$

The turbulence intensity levels are also found to be higher for higher air gap height as shown in Figure 11. This is further evidenced in Figure 12 which shows the variation of heat transfer coefficient for the non-dimensional distance of the absorber plate between two consecutive deflector ribs. It is seen that the height value of 10mm has greater value of heat transfer coefficient between consecutive ribs as compared to other height values which is due to the contact of relatively fast moving core flow with that of the absorber plate for the entire inter-rib distance.



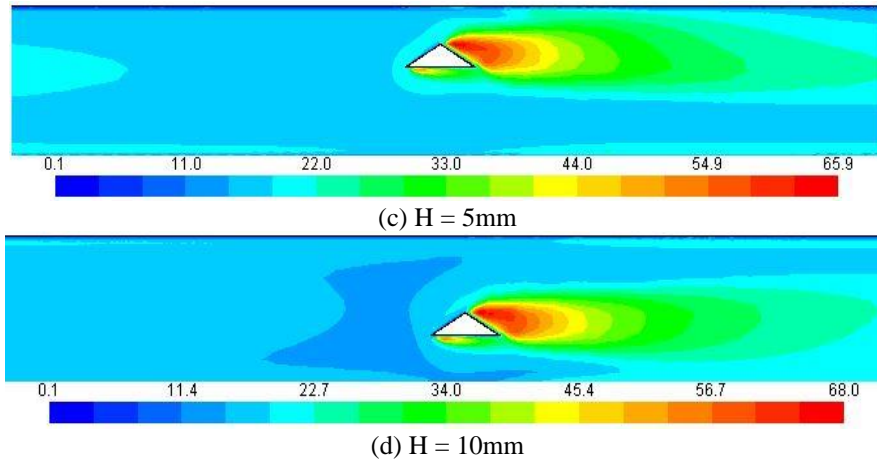


Figure 11. Comparison of turbulence intensity for different heights at a fixed pitch value of 160 mm for the non-dimensional test section length of $X/L=0.025$ to $X/L=0.15$

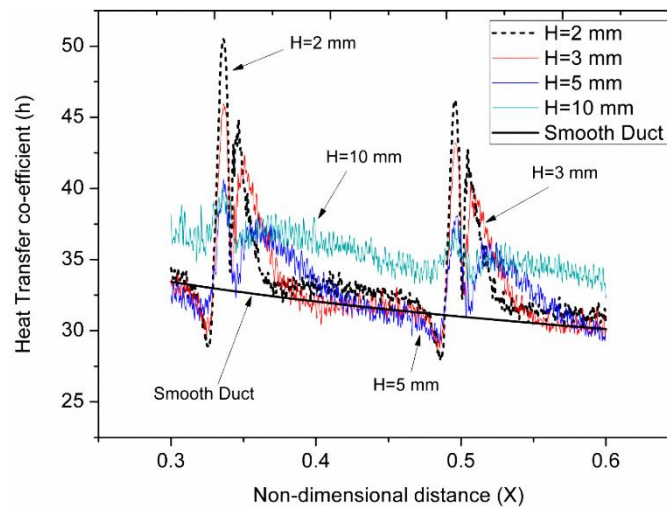


Figure 12. Comparison of heat transfer coefficient for non-dimensional distance of the absorber plate between two consecutive deflector ribs for different air gap heights

Effect of Air Gap Height Variation on Friction Factor Characteristics

The variation of friction factor for different air gap heights with reference to smooth duct is shown Figure 13. The friction factor is seen to be higher for larger air gap heights which can be due to the fact that greater height values increase the flow obstruction. As the air gap height increases, the rib moves much deeper into the core flow where the fluid velocity is at its peak leading to increased flow obstruction.

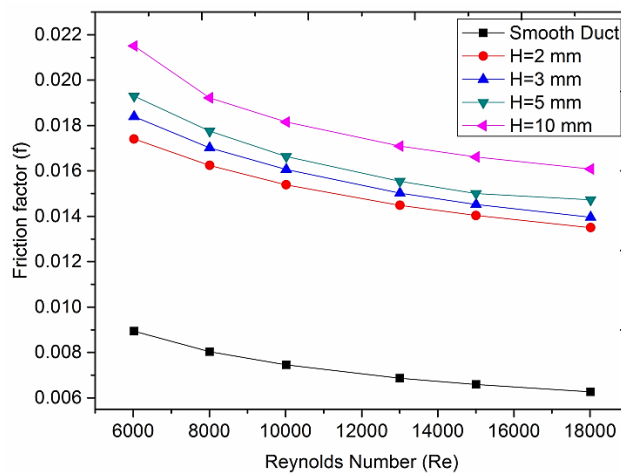


Figure 13. Comparison of friction factor for different air gap height values for a fixed deflector rib pitch of 160 mm

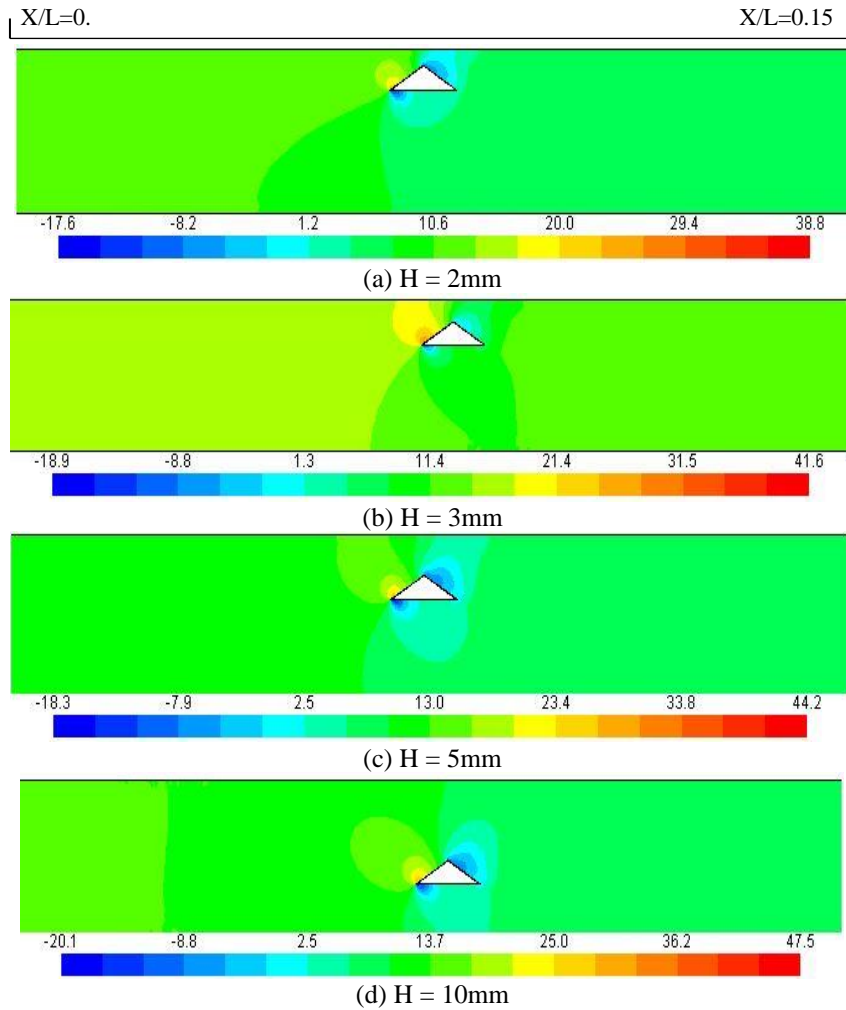


Figure 14. Comparison of pressure distribution across the rib for different heights at a fixed pitch value of 320 mm for the non-dimensional test section length of $X/L=0.025$ to $X/L=0.15$

As the high velocity flow hits the rib and gets deflected, the local pressure on the upstream side of the deflector increases due to energy loss while the pressure on the downstream of the rib decreases due to fast moving air thereby increasing the pressure drop across the rib as shown by the pressure contour plots in Figure 14. The friction factor increase was found to be as high as 2.56 times the smooth duct for the height value of 10mm at $Re=18000$.

Thermal Enhancement Factor

The variation of thermal enhancement factor for different pitch values of 40mm, 80mm, 160mm and 320mm for a fixed air gap height of 3mm is shown in Figure 15. The thermal enhancement factor is given by:

$$TEF = \frac{Nu_r / Nu}{[f_r / f]^{1/3}} \quad (10)$$

It is seen that the thermal enhancement factor is greater for lower pitch values. This is due to a significantly higher friction factor at lower pitch values as compared to higher pitch values. Though, the Nusselt number increase is relatively higher for lower pitch values, the corresponding increase in friction factor is also found to be significant. As a result, the effective thermal performance as indicated by thermal enhancement factor is also lower. In fact, it is lesser than 1.0 for the pitch value of 40mm and 80 mm for all the Reynolds number conditions used in the analysis. The pitch values of 160mm is found to exhibit the thermal enhancement factor greater than 1.0 for flow Reynolds number less than 8000 while the pitch value of 320 mm exhibits thermal enhancement factor greater than 1.0 for all the Reynolds number used in the analysis. Thus, for a given height of 3mm, a pitch value of 320mm is effective in providing enhanced heat transfer.

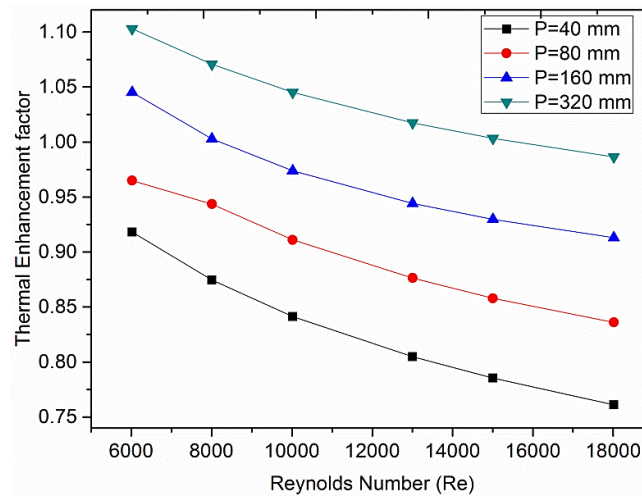


Figure 15. Comparison of thermal enhancement factor for different deflector rib pitch values for a fixed air gap height of 3 mm

Figure 16 shows the comparison of thermal enhancement factor for varying height values at a fixed pitch of 160mm. It is seen that lower height values exhibit greater thermal enhancement factor. This is due to greater flow obstructions offered by higher air gap heights although are capable of producing increased heat transfer. Lower height values are found to have greater useful range of flow rates where the thermal enhancement factor is maintained greater than 1.0. The useful range of Reynolds number for which the deflector rib can be used for enhancing the heat transfer decreases with increase in height values. The air gap height value of 10mm exhibits a thermal enhancement factor lesser than 1.0 and hence is not recommendable for use as heat transfer enhancement device for the entire Reynolds number range used in the analysis.

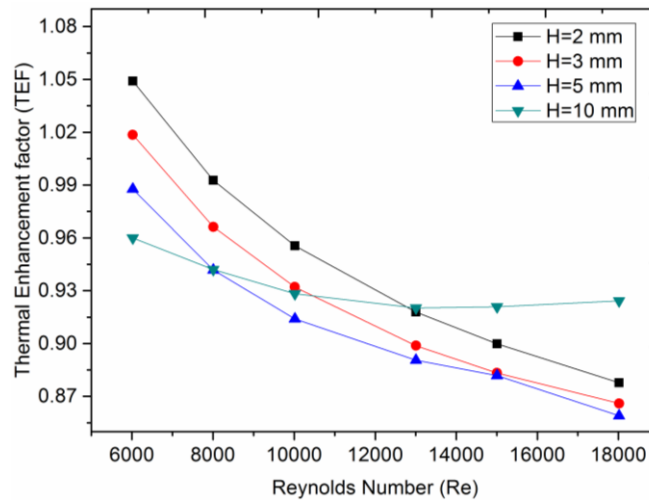


Figure 16. Comparison of thermal enhancement factor for different air gap heights for a fixed deflector rib pitch value of 160 mm

CONCLUSIONS

A two-dimensional CFD analysis is carried out to evaluate the effect of ribs on the effective thermal performance of solar air heater for different Reynolds number. The deflector plate of triangular cross-section is chosen in the analysis and the effect of air gap height as well as the number of deflector ribs on the overall thermal performance of solar air heater is brought out using two-dimensional CFD analysis under constant heat flux conditions. The analysis leads to the following conclusions:

- The presence of deflector ribs provides augmented heat transfer through flow acceleration and enhanced turbulence levels.
- The Nusselt number increase is as high as 1.39 times in comparison to smooth duct for the pitch value of 40mm and air gap height of 3mm.
- The highest increase in friction factor is found to be 3.82 times that of smooth duct for pitch value of 40mm and air gap height of 3mm.

- The highest thermal enhancement factor is achieved for the pitch value of 320mm and air gap height of 3mm at $Re=6000$.
- The air gap height value of 10mm exhibits thermal enhancement factor lesser than 1.0 and hence is not recommended for use as heat transfer enhancement device for the entire Reynolds number range used in the analysis
- The pitch value of 320 mm exhibits thermal enhancement factor greater than 1 for almost all the Reynolds number range used in the analysis and varies between 0.93 and 1.07.

The deflector rib cross-sectional geometry will significantly influence the flow behaviour and heat transfer and needs to be studied in detail as future scope for research.

ACKNOWLEDGEMENTS

We would like to thank Manipal Academy of higher Education, Dubai Campus, Dubai for providing the computational facility to carry out the simulation work. The authors also thankfully acknowledge the facilities provided by the Manipal Institute of Technology, Manipal, India for carrying out this work.

REFERENCES

- [1] M. Ansari and M. Bazargan, "Optimization of flat plate solar air heaters with ribbed surfaces," *Appl. Therm. Eng.*, vol. 136, no. November 2016, pp. 356–363, 2018.
- [2] A. S. Abdullah, M. M. Abou Al-sood, Z. M. Omara, M. A. Bek, and A. E. Kabeel, "Performance evaluation of a new counter flow double pass solar air heater with turbulators," *Sol. Energy*, vol. 173, no. February, pp. 398–406, 2018.
- [3] I. Singh, S. Vardhan, S. Singh, and A. Singh, "Experimental and CFD analysis of solar air heater duct roughened with multiple broken transverse ribs: A comparative study," *Sol. Energy*, vol. 188, no. June, pp. 519–532, 2019.
- [4] D. Jin, S. Quan, J. Zuo, and S. Xu, "Numerical investigation of heat transfer enhancement in a solar air heater roughened by multiple V-shaped ribs," *Renew. Energy*, vol. 134, pp. 78–88, 2019.
- [5] C. A. Komolafe, I. O. Oluwaleye, O. Awogbemi, and C. O. Osueke, "Experimental investigation and thermal analysis of solar air heater having rectangular rib roughness on the absorber plate," *Case Stud. Therm. Eng.*, vol. 14, no. February, p. 100442, 2019.
- [6] R. Kumar, V. Goel, and A. Kumar, "Investigation of heat transfer augmentation and friction factor in triangular duct solar air heater due to forward facing chamfered rectangular ribs: A CFD based analysis," *Renew. Energy*, vol. 115, pp. 824–835, 2018.
- [7] D. S. Thakur, M. K. Khan, and M. Pathak, "Performance evaluation of solar air heater with novel hyperbolic rib geometry," *Renew. Energy*, vol. 105, pp. 786–797, 2017.
- [8] M. N. Manjunath M S, Venkatesh R, "Thermal performance enhancement of flat plate solar air heater using transverse U-shaped turbulator - A numerical study," *J. Mech. Eng. Sci.*, vol. 2, no. 3, pp. 212–214, 2019.
- [9] Y. Menni, A. Azzi, and A. J. Chamkha, "Optimal thermo aerodynamic performance of s-shaped baffled channels," *J. Mech. Eng. Sci.*, vol. 12, no. 3, pp. 3888–3913, 2018.
- [10] M. S. Manjunath, K. V. Karanth, and N. Y. Sharma, "Numerical investigation on heat transfer enhancement of solar air heater using sinusoidal corrugations on absorber plate," *Int. J. Mech. Sci.*, vol. 138–139, no. January, pp. 219–228, 2018.
- [11] G. K. Poongavanam, K. Panchabikesan, A. J. D. Leo, and V. Ramalingam, "Experimental investigation on heat transfer augmentation of solar air heater using shot blasted V-corrugated absorber plate," *Renew. Energy*, vol. 127, pp. 213–229, 2018.
- [12] H. Zhang *et al.*, "Mathematical modeling and performance analysis of a solar air collector with slit-perforated corrugated plate," *Sol. Energy*, vol. 167, no. April, pp. 147–157, 2018.
- [13] M. T. Baissi, A. Brima, K. Aoues, R. Khanniche, and N. Moumimi, "Thermal behavior in a solar air heater channel roughened with delta-shaped vortex generators," *Appl. Therm. Eng.*, vol. 165, no. August 2018, p. 113563, 2020.
- [14] S. Skullong, P. Promthaisong, P. Promvong, C. Thianpong, and M. Pimsarn, "Thermal performance in solar air heater with perforated-winglet-type vortex generator," *Sol. Energy*, vol. 170, no. August 2017, pp. 1101–1117, 2018.
- [15] K. Rajarajeswari, P. Alok, and A. Sree Kumar, "Simulation and experimental investigation of fluid flow in porous and non-porous solar air heaters," *Sol. Energy*, vol. 171, no. April, pp. 258–270, 2018.
- [16] A. Heydari and M. Mesgarpour, "Experimental analysis and numerical modeling of solar air heater with helical flow path," *Sol. Energy*, vol. 162, no. January, pp. 278–288, 2018.
- [17] M. S. Manjunath, K. V. Karanth, and N. Y. Sharma, "Numerical Analysis of Flat Plate Solar Air Heater Integrated With an Array of Pin Fins on Absorber Plate for Enhancement in Thermal Performance," vol. 141, no. October, pp. 1–12, 2019.
- [18] J. P. Tsia and J. J. Hwang, "Measurements of heat transfer and fluid flow in a rectangular duct with alternate attached-detached rib-arrays," *Int. J. Heat Mass Transf.*, vol. 42, no. 11, pp. 2071–2083, 1998.
- [19] K. Yongsiri, P. Eiamsa-Ard, K. Wongcharee, and S. Eiamsa-Ard, "Augmented heat transfer in a turbulent channel flow with inclined detached-ribs," *Case Stud. Therm. Eng.*, vol. 3, pp. 1–10, 2014.

- [20] J. L. Bhagoria, J. S. Saini, and S. C. Solanki, "Heat transfer coefficient and friction factor correlations for rectangular solar air heater duct having transverse wedge shaped rib roughness on the absorber plate," *Renew. Energy*, vol. 25, no. 3, pp. 341–369, 2002.
- [21] A. S. Yadav and J. L. Bhagoria, "A numerical investigation of square sectioned transverse rib roughened solar air heater," *Int. J. Therm. Sci.*, vol. 79, pp. 111–131, 2014.
- [22] A. S. Yadav and J. L. Bhagoria, "A numerical investigation of turbulent flows through an artificially roughened solar air heater," *Numer. Heat Transf. Part A Appl.*, vol. 65, no. 7, pp. 679–698, 2014.